Tellus (2003), 55A, 219–231
Printed in UK. All rights reserved

TELLUS
ISSN 0280–6495

Nonhydrostatic generalization of a pressure-coordinate-based hydrostatic model with implementation in HIRLAM: validation of adiabatic core

By AARNE MÄNNIK*, REIN RÕÕM and ANDRES LUHAMAA, *Institute of Environmental Physics, Tartu University, Ülikooli 18, 50090 Tartu, Estonia*

(Manuscript received 26 February 2002; in final form 14 January 2003)

ABSTRACT

A nonhydrostatic pressure-coordinate model of atmospheric dynamics is developed. The model filters acoustic mode. Internal acoustic waves are filtered using the assumption of non-divergence of motion in pressure-space. External (Lamb mode) waves are filtered using the surface pressure adjustment. The model is implemented in the framework of the numerical weather prediction model HIRLAM (High Resolution Limited Area Model) as an extension to the hydrostatic kernel. The integration scheme is either the explicit or semi-implicit Eulerian leapfrog time stepping. Due to the acoustic filtration, the explicit scheme supports quite large time-steps. To check the validity of the model, several flow experiments with artificial orography are performed. The hydrostatic and nonhydrostatic flow regimes are investigated. The results of different models are compared mutually and with the analytic solutions. The real situation simulations are also presented to show the model's forecasting capabilities.

1. Introduction

Driven by the growth of computational resources, interest in the application of nonhydrostatic models for numerical weather prediction has grown substantially during the past decade. Nonhydrostatic models have been used for scientific purposes for a long time, while weather forecasting has traditionally been the domain of hydrostatic models. In recent years, the situation has started to change. The nonhydrostatic Lokal-Modell of the Deutsche Wetterdienst is in operational use since 1999. The Mesoscale Prediction Group at NCAR runs MM5 (Dudhia, 1993) operationally. To support research, nonhydrostatic models UW-NMS (Tripoli, 1992) and MM5 are implemented for the operational real-time short range forecast by the University of Wisconsin-Madison, University of Washington, and various other universities and organizations. Many weather prediction centers in the world are investigating the possible application of operational forecasting with nonhydrostatic models (Carpenter, 1979; Bubnova et al., 1995; Tanguay et al., 1990; Yeh et al., 2002).

The increasing resolution and nonhydrostatic equations pose new challenges to the future weather forecasting, raising unsolved problems for parameterization of the physics and data assimilation cycle, and introducing new paradigms to forecast interpretations.

Most of the current operational weather forecasting models are based on the hydrostatic primitive equations with the terrain-following, pressure-based vertical coordinate. It would be advantageous to have direct extensions of these models into the nonhydrostatic domain. The shortcut extension would minimize the development effort, and it would have an additional advantage of maintaining the analysis,

*Corresponding author.
e-mail: aarne.mannik@ut.ee

post-processing and verification tools and packages. One such approach is described in this paper, and its practical implementation in the existing numerical weather prediction model is explained.

Pressure coordinates for the hydrostatic models were introduced by Eliassen (1949). The first nonhydrostatic model in pressure coordinates was presented by Miller (1974) and Miller and Pearce (1974), followed by generalizations by White (1989) and Salmon and Smith (1994). Those models were developed by extending the hydrostatic equations with the equations describing nonhydrostatic effects while maintaining the condition of non-divergence of motion in pressure-space. The full set of equations in pressure coordinates, describing atmospheric motions and limits of their application, was presented by Rõõm (1990). A close approach was developed by Laprise (1992), who employed hydrostatic pressure as the vertical coordinate, and Dudhia (1993), who used the hydrostatic mean background pressure for the vertical coordinate.

In this research, the White model, complemented with the assumption of the surface pressure adjustment (Rõõm, 2001) is used to extend the hydrostatic equations into the nonhydrostatic domain. In the White model, the assumption of incompressibility of the medium in pressure space takes care of the internal acoustic wave filtration. To get a completely anelastic model, the assumption of surface pressure adjustment is applied, which eliminates the external acoustic waves (the so-called Lamb mode). With the complete acoustic filtration, much larger time steps are available during numerical integration, which is very important if we bear in mind how demanding the nonhydrostatic models are with respect to computational resource requirements. This approach has previously been tested in the nonhydrostatic model NH3D (Rõõm et al., 2001).

HIRLAM (High Resolution Limited Area Model) is used as the hydrostatic parent-model. HIRLAM is the joint effort of several European countries to develop a high resolution limited area weather forecasting model. In these countries, HIRLAM is used for routine weather prediction in close cooperation with ECMWF. The hydrostatic HIRLAM can currently use the explicit or semi-implicit Eulerian (Robert et al., 1972) and the semi-implicit semi-Lagrangian (Robert, 1982) time integration schemes. The variety of options makes HIRLAM an attractive platform for the development and comparison of different nonhydrostatic models.

An overview of the nonhydrostatic HIRLAM is introduced below. Only the nonhydrostatic extension of the adiabatic core is described, whereas the physical routines of HIRLAM are left out of consideration, as they remain untouched. Dynamic equations are presented with the emphasis on the nonhydrostatic modifications of the hydrostatic model, and the details of numerical implementation are described in section 2. Performance tests and model comparisons are presented in section 3 with the emphasis on adiabatic core behavior.

2. Model

2.1. Diagnostic relations

HIRLAM is implemented in the rotated spherical coordinates system (λ, θ), but in the present formulation the pseudo-planar coordinates $x = a\lambda$, $y = a\theta$ are used, where a is the mean radius of the Earth. The physical coordinates (X, Y) are related to these as $X = h_x x$, $Y = h_y y$, where the metric coefficients are $h_x = \cos\ \theta$, $h_y = 1$. The use of x and y enables the most symmetric presentation of gradient and divergent operators.

Vertically, HIRLAM has the hybrid-pressure coordinate η (Simmons and Burridge, 1981). The coordinate surfaces follow the terrain near the bottom, and on the upper levels they transform into pressure coordinates. The nonhydrostatic model continues to use the same vertical coordinate system with a small difference introduced from the ideology of the surface pressure adjustment. Instead of the actual surface pressure p_s, a background surface pressure field $\overline{p}_s(\mathbf{x}, t)$ is used. The integration domain is a segment of the spherical layer with flat top at $p = 0$ and uneven bottom $p = \overline{p}_s(\mathbf{x}, t)$:

$$-\Lambda < \lambda < \Lambda, \quad -\Theta < \theta < \Theta, \quad 0 < p < \overline{p}_s(\mathbf{x}, t).$$

With the help of weights $A(\eta)$ and $B(\eta)$ the pressure coordinate presents as $p = A + B\overline{p}_s$. The background pressure field can be fixed in time or be externally driven by a nesting model. For convenience, the density in hybrid coordinates is introduced

$$m = \frac{\partial p}{\partial \eta}.$$

The "horizontal" hybrid-coordinate gradient and divergence differential operators in spherical coordinates are, respectively,

$$\nabla a = \mathbf{i}^x \frac{1}{h_x}\frac{\partial a}{\partial x} + \mathbf{i}^y \frac{1}{h_y}\frac{\partial a}{\partial y},$$

$$\nabla \cdot \mathbf{a} = \frac{1}{h_x h_y}\left(\frac{\partial h_y a_x}{\partial x} + \frac{\partial h_x a_y}{\partial y}\right).$$

Using these operators, the "horizontal" gradient and divergence operators on the pressure surfaces are introduced

$$\widehat{\mathbf{G}}a = \nabla a - \frac{1}{m}\frac{\partial a}{\partial \eta}\nabla p$$

$$\widehat{\mathbf{G}}^{+} \cdot \mathbf{a} = \nabla \cdot \mathbf{a} - \frac{1}{m}\frac{\partial \mathbf{a}}{\partial \eta} \cdot \nabla p.$$

The full geopotential Φ consists of thermic and baric components φ and ϕ:

$$\Phi = \varphi + \phi,$$

where the thermic geopotential is, in essence, the same as the hydrostatic geopotential of the common hydrostatic model:

$$\varphi = gh + \int_{\eta}^{1} RT\frac{m d\eta'}{p},$$

where h is the surface elevation, R is the gas constant, T is the absolute temperature and g is the gravitational acceleration. The only difference between the present and common definitions of φ is that the hydrostatic model uses the actual hydrostatic surface pressure p_s instead of the background pressure $\overline{p}_s$ in computations. The baric geopotential ϕ represents the additional contribution, which arrives at the nonhydrostatic pressure coordinate dynamics.

A special novel feature of the model is that the surface pressure is treated as an adjusted one. That means that the surface pressure is not a prognostic variable anymore. Instead, it is diagnosed from the distribution of the baric geopotential at the lowest level. The actual surface pressure consists of the mean, steady component, and the small adjusted contribution p'_s:

$$p_s = \overline{p}_s + p'_s.$$

The steady part $\overline{p}_s$ is pre-specified; in practice it is taken from the time-interpolated boundary fields. The fluctuating part is diagnosed from the formula

$$p'_s = \overline{p}_s\left(\frac{\phi}{RT}\right)_{\overline{p}_s}.$$

A detailed description of obtaining this diagnostic relation is given by Rõõm (2001).

2.2. Dynamic equations

The adiabatic core of the nonhydrostatic model is described below. The nonhydrostatic model is based on the Eulerian equations of motion of the hydrostatic HIRLAM, which in turn are the limited area version of the ECMWF global hybrid-coordinate, primitive equation model. As mentioned in the introduction, the presented model is essentially the numerical realization of the White (1989) model with a surface pressure adjustment assumption. Thus, an approach has been chosen which concentrates on a description of the actual extension technique and omits a detailed examination of dynamic details. The following nonhydrostatic formulation of the equations is discrete in time, while the spatial representation remains continuous. The approach is very suitable for the description of the model, allowing for a compact presentation of both the nonhydrostatic and implicit features as moderate extensions to the basic hydrostatic primitive equations. Emphasis is put on the semi-implicit nonhydrostatic formulation. Derivation of the explicit model from these equations is straightforward and is presented later.

With the notation

$$X^t = X(t), \quad \partial_t X = \frac{X^{t+\Delta t} - X^{t-\Delta t}}{2\Delta t},$$

$$\overline{X}^t = \frac{X^{t+\Delta t} + X^{t-\Delta t}}{2},$$

$$\Delta_{tt} X = \frac{1}{2}(X^{t+\Delta t} + X^{t-\Delta t}) - X^t,$$

the basic model equations are as follows:

$$\frac{\partial \mathbf{v}}{\partial t} = \mathbf{F}_{\mathbf{v}} - \widehat{\mathbf{G}}\overline{\phi}^t - \widehat{\mathbf{G}}\Delta_{tt}\varphi, \tag{2.2.1}$$

$$\partial_t T = F_T + S^t \Delta_{tt}\omega, \tag{2.2.2}$$

$$\widehat{\mathbf{G}}^{+} \cdot \mathbf{v}^t + \frac{1}{m}\frac{\partial \omega^t}{\partial \eta} = 0, \tag{2.2.3}$$

$$\frac{\partial \varphi}{\partial \eta} = \frac{mRT}{p} \tag{2.2.4}$$

$$\mathcal{L}\overline{\phi}^t + \widehat{\mathbf{G}}^{+} \cdot \widehat{\mathbf{G}}(\Delta_{tt}\varphi) = A^v, \tag{2.2.5}$$

where $\mathbf{v} = \{u, v\}$ is the horizontal velocity vector, ϕ is the baric geopotential, $\mathcal{L}$ is the elliptic operator

$$\mathcal{L}\overline{\phi}^t \equiv \widehat{\mathbf{G}}^+ \cdot \widehat{\mathbf{G}}\overline{\phi}^t + \frac{1}{m}\frac{\partial}{\partial \eta}\left(\frac{p^2}{mH^2}\frac{\partial \overline{\phi}^t}{\partial \eta}\right) \tag{2.2.6}$$

and

$$A^v = \widehat{\mathbf{G}}^+ \cdot \mathbf{F}_\mathbf{v} + \frac{1}{m}\frac{\partial F_\omega}{\partial \eta} \tag{2.2.7}$$

is the source function.

Equations (2.2.1)–(2.2.5) present the momentum tendency equation, temperature tendency equation, continuity equation, hydrostatic equation for thermic geopotential and diagnostic equation for baric geopotential, respectively. $\mathbf{F}_\mathbf{v}$ and F_T are the hydrostatic tendencies, which are exactly the same as in the hydrostatic case:

$$\mathbf{F}_\mathbf{v} = (f + \xi)\mathbf{i}^z \times \mathbf{v} - \dot{\eta}\frac{\partial \mathbf{v}}{\partial \eta} - RT\nabla(\ln p) + \nabla(\varphi + E) + \mathbf{P}_\mathbf{v} + \mathbf{K}_\mathbf{v}, \tag{2.2.8}$$

$$F_T = -\mathbf{v}\cdot\nabla T - \dot{\eta}\frac{\partial T}{\partial \eta} + \frac{RT\omega}{c_p p} + P_T + K_T, \tag{2.2.9}$$

where c_p is the heat capacity at constant pressure. The vorticity and energy terms are

$$\xi = \frac{1}{h_x h_y}\left(\frac{\partial h_y v}{\partial x} - \frac{\partial h_x u}{\partial y}\right), \tag{2.2.10}$$

$$E = \frac{1}{2}\left(u^2 + v^2\right), \tag{2.2.11}$$

and P- and K-terms represent the tendencies from physical parameterization and horizontal diffusion, respectively. It is essential to underline that the equation set (2.2.1)–(2.2.11) is actually very close to the system of common hydrostatic, primitive equations, employed in the hydrostatic HIRLAM. Without the gradient term $\widehat{\mathbf{G}}\overline{\phi}^t$ in eq. (2.2.1) and the terms with operator Δ_{tt} in eqs. (2.2.1) and (2.2.2), eqs. (2.2.1)–(2.2.4) together with (2.2.8)–(2.2.11) would represent the explicit hydrostatic primitive equation model. The only exception from the hydrostatic model is the geopotential φ, which in the nonhydrostatic case means the thermic geopotential rather than the hydrostatic one. The term

$$S = \frac{RT}{c_p p} - \frac{1}{m}\frac{\partial T}{\partial \eta}$$

in the temperature equation characterizes the stratification stability, and H in eq. (2.2.6) is the scale height defined as $H = RT/g$. Note that parameters S and H are treated on the time level t

$$S \equiv S^t, \quad H \equiv H^t.$$

For the deduction of the elliptic equation for the baric geopotential ϕ, the equation of vertical momentum is required, which exposes in hybrid coordinates as

$$\frac{\partial \omega}{\partial t} = F_\omega - \frac{p^2}{mH^2}\frac{\partial \overline{\phi}^t}{\partial \eta}, \tag{2.2.12}$$

$$F_\omega = -\mathbf{v}\cdot\nabla\omega - \dot{\eta}\frac{\partial \omega}{\partial \eta} + \omega\left(\frac{c_v}{c_p}\frac{\omega}{p} - \frac{K_T}{T} - \frac{P_T}{T} - \frac{1}{R}\frac{\mathrm{d}R}{\mathrm{d}t}\right) + K_\omega + P_\omega, \tag{2.2.13}$$

where c_v is the heat capacity at constant volume. R would be time dependent only if the moist physics is included. Elliptic equation (2.2.5) can be derived by differentiating the continuity equation (2.2.3) in time and eliminating velocity tendencies from eqs. (2.2.1) and (2.2.12).

Terms $\Delta_{tt}\omega$ and $\Delta_{tt}\varphi$ describe the numerical effect of the implicit time integration scheme. The terms appear from numerical discretization in time and they have a stabilizing effect in computations. Their derivation is presented in the Appendix, and the terms are specified via ϕ as follows:

$$\Delta_{tt}\omega = -\Delta t\left(\frac{p}{H}\right)^2\frac{\partial \overline{\phi}^t}{m\partial \eta} + \mu_\omega, \tag{2.2.14}$$

$$\Delta_{tt}\varphi = -\Delta t^2\int_\eta^1 N^2\frac{\partial \overline{\phi}^t}{\partial \eta}d\eta + Q, \tag{2.2.15}$$

where

$$Q = R\int_\eta^1(\mu_T + \Delta t S\mu_\omega)\frac{m}{p}\mathrm{d}\eta,$$

$$\mu_\omega = \Delta t F_\omega^t - \omega^t + \omega^{t-\Delta t},$$

$$\mu_T = \Delta t F_T^t - T^t + T^{t-\Delta t},$$

and N represents the Brunt–Väisälä frequency:

$$N^2 = \frac{RSp}{H^2}. \tag{2.2.16}$$

The system of explicit equations is obtained by omitting $\Delta_{tt}\omega$ and $\Delta_{tt}\varphi$ in eqs. (2.2.1), (2.2.2) and

(2.2.5). It corresponds to the case $\Delta t \rightarrow 0$, when the difference between the explicit and semi-implicit equations vanishes. Thus, the explicit model is a subset of semi-implicit equations.

The hydrostatic HIRLAM uses the Davies (1976) boundary relaxation zone, where the modeled meteorological fields are relaxed toward the values from the nesting model near the lateral boundaries. This approach is reasonable for limited area models, and the nonhydrostatic HIRLAM implements it as well. Meanwhile, in the nonhydrostatic case, the boundary conditions for elliptic equation (2.2.5) have to be additionally specified. The application of the Davies boundary relaxation zone dictates the use of the Neumann condition

$$\left(\frac{\partial \phi}{\partial n}\right)_\Gamma = 0, \tag{2.2.17}$$

as the only possible choice. For the upper and lower boundaries, the nonhydrostatic model has no fixed boundary conditions for ϕ. Instead, the baric geopotential evolves freely at the bottom and top boundaries. However, this evolution is still controlled by two integral conditions. One condition arises from the assumption of the ground surface pressure adjustment and expresses in η-coordinates as

$$\nabla \cdot \int_0^1 (\widehat{\mathbf{G}}\phi) m \, \mathrm{d}\eta = \nabla \cdot \int_0^1 \mathbf{F}_\mathrm{v} m \, \mathrm{d}\eta. \tag{2.2.18}$$

The second one is the integrability condition

$$\int_0^1 |\phi| m \, \mathrm{d}\eta < \infty \quad \text{if} \quad \int_0^1 |A^v| m \, \mathrm{d}\eta < \infty, \tag{2.2.19}$$

which eliminates solutions of the homogeneous equation $\mathcal{L}\phi = 0$ that grow exponentially with height from consideration. Conditions (2.2.18) and (2.2.19) specify the solution uniquely at every instant.

2.3. *Numerics*

2.3.1. Implementation details. A comprehensive description of the numerical representation can be found in Männik and Rõõm (2001) and Rõõm and Männik (2002). As the model is implemented in the framework of HIRLAM, the major part of the numerics has been inherited from the hydrostatic base model. The grid has the classical C-type (Arakawa and Lamb, 1997) staggering of horizontal velocity variables with respect to the scalars. In the vertical the staggering scheme by Simmons and Burridge (1981) is used. Scalar fields like the temperature T, the baric geopotential ϕ, etc., are located between the levels of the vertical velocity ω. The exception is the thermic geopotential φ, which is located on the same levels as ω.

The nonhydrostatic model leads to small modifications in the existing routines of the dynamics. The computation of the vertical velocity field is required to supply the source function (2.2.7) with the vertical derivative of the vertical velocity tendency. A minor modification is introduced by the usage of the thermic geopotential instead of the hydrostatic one. A small update to the energy conversion term in eq. (2.2.2) is required to keep the energy conservation consistent. However, all these modifications are minor changes in the existing routines of hydrostatic dynamics.

The biggest modification in comparison with the hydrostatic model is caused by the introduction of the baric geopotential ϕ and elliptic equation (2.2.5). The elliptic solver is an essential part of the nonhydrostatic code and its numerical quality is crucial to the whole model. The solver is based on the use of the three-dimensional orthogonal basis: the three-dimensional basis is presented as the multiplication of the three one-dimensional bases. In horizontal directions the discrete cosine-Fourier bases are employed. In the vertical, the eigenvectors of the horizontally homogenized vertical part:

$$\mathcal{L}_p = \frac{1}{\langle m \rangle} \frac{\partial}{\partial \eta} \left\langle \frac{p^2}{m H^2} \right\rangle \frac{\partial}{\partial \eta}$$

of the operator (2.2.6) are used. $\langle\,\rangle$ denote the operator of averaging along η-surfaces. The elliptic operator (2.2.6) is divided into the main part and the perturbation operator. The main part, which is the horizontally homogenized Laplacian, is inverted explicitly using the orthogonal basis, whereas the perturbation part is iterated. Normally, two or three iterations are required.

An important simplification is used by the semi-implicit scheme, where N is approximated with a constant (approximately equal to the mean value over the integration domain) in eq. (2.2.15). Such simplification has a strong influence on the stability of the scheme. The sphericity of the Earth is treated as a perturbation to the plain geometry. This sets some limitations on the horizontal extent of the domain of integration. In practice, the areas exceeding 5000 km along side should not be used.

Table 1. *Time-steps of the nonhydrostatic model*

Δx (km)	a_0 (km)	$U_{\max}$ (m s^{-1})	$\frac{\Delta x}{U_{\max}}$(s)	Time-step of explicit model (s)	Time-step of semi-implicit model (s)
11	30	30	366.7	60	340
5.5	10	30	183	40	180
0.55	10	30	18.3	14	17
0.55	2.5	30	18.3	16	18

2.3.2. Practical details. As a result of the complete filtration of acoustic waves the explicit implementation of the model can have a much longer time-step than the unfiltered explicit models. The time-step of the explicit scheme is determined by the speed of internal buoyancy waves, whereas the time-step of the semi-implicit scheme is mainly determined by the speed of advection.

Time-steps of the explicit and semi-implicit implementations of the nonhydrostatic model in several artificial flow situations with different resolutions Δx are presented in Table 1. The flow over a 2D mountain profile is modeled, characterized by the half-width a_0 and the maximum wind $U_{\max}$.

As expected, the semi-implicit implementation has time-steps close to the theoretical estimate $\Delta x/U_{\max}$. It is seen from Table 1 that the difference between different implementations diminishes at higher resolutions, where the speed of buoyancy waves decreases. Despite the smaller time-step, the explicit model is favorable in situations, where the correct representation of waves is required, as the semi-implicit scheme tends to distort the phase speed of the disturbances. Thus, the explicit filtered model is an attractive choice for high-resolution modeling.

From the point of view of the numerical efficiency, the non-hydrostatic model spends roughly 20% more time on time-steps than the semi-implicit Eulerian hydrostatic model, but the differences are implementation-specific. Due to the larger time-step the explicit non-hydrostatic model is significantly more efficient than the explicit hydrostatic model.

In addition to the existing fourth-order spectral smoothing, implemented in the hydrostatic HIRLAM, the nonhydrostatic model introduces a top sponge layer, which is based on the second-order spectral smoothing. The smoothing coefficient increases near the top to achieve the effective dissipation of the energy released by the upward propagating disturbances. This second-order smoothing is optional for the semi-implicit scheme, but necessary in the explicit case.

3. Validation results

3.1. Experiments with artificial orography

Experimentation with the adiabatic flows over hills is the traditional approach to the model quality testing. Well known semi-analytic solutions exist for linear flow regimes and they can be used for comparison. The steady flow with the constant wind speed $u = U$ over the hill in the stably stratified atmosphere is modeled. The orography is chosen to be a bell-shaped mountain ridge with the profile $h = h_0/(1 + x^2/a_x^2 + y^2/a_y^2)^{3/2}$, where h_0 is the maximum mountain height and a_x, a_y are the half-widths along the coordinate axes. This profile is known as the "Witch of Agnesi" mountain. The stratification of the atmosphere is described with the constant Brunt–Väisälä frequency N.

Three experiments of the flow over obstacles with different resolutions are presented below. The purpose is to demonstrate that the nonhydrostatic model gives reliable results and can describe the nonhydrostatic phenomena. Both the explicit and semi-implicit realizations are compared to the semi-analytic solution and the hydrostatic semi-implicit Eulerian model. In the first two experiments the mountain used is two-dimensional, in the sense that the half-width a_y is infinite.

In the first experiment, the mountain has the height $h_0 = 250$ m and the half-width $a_x = 30$ km. The flow speed is $U = 25$ m s^{-1}, and the atmosphere is isothermal with the Brunt–Väisälä frequency $N = 0.018$ s^{-1}. A dimensionless parameter Nh/U is often used (Laprise and Peltier, 1989; Baines, 1995) to characterize the flow properties. In the current case $Nh/U = 0.18$, which is small enough to assume the linearity of the flow. The second well known parameter Na_x/U is a valid indicator of the nonhydrostatic character of the flow. For the first experiment its value is much larger than 1, which corresponds to the hydrostatic flow regime. Figure 1 shows the results of 6 h integrations with different models, the explicit nonhydrostatic,

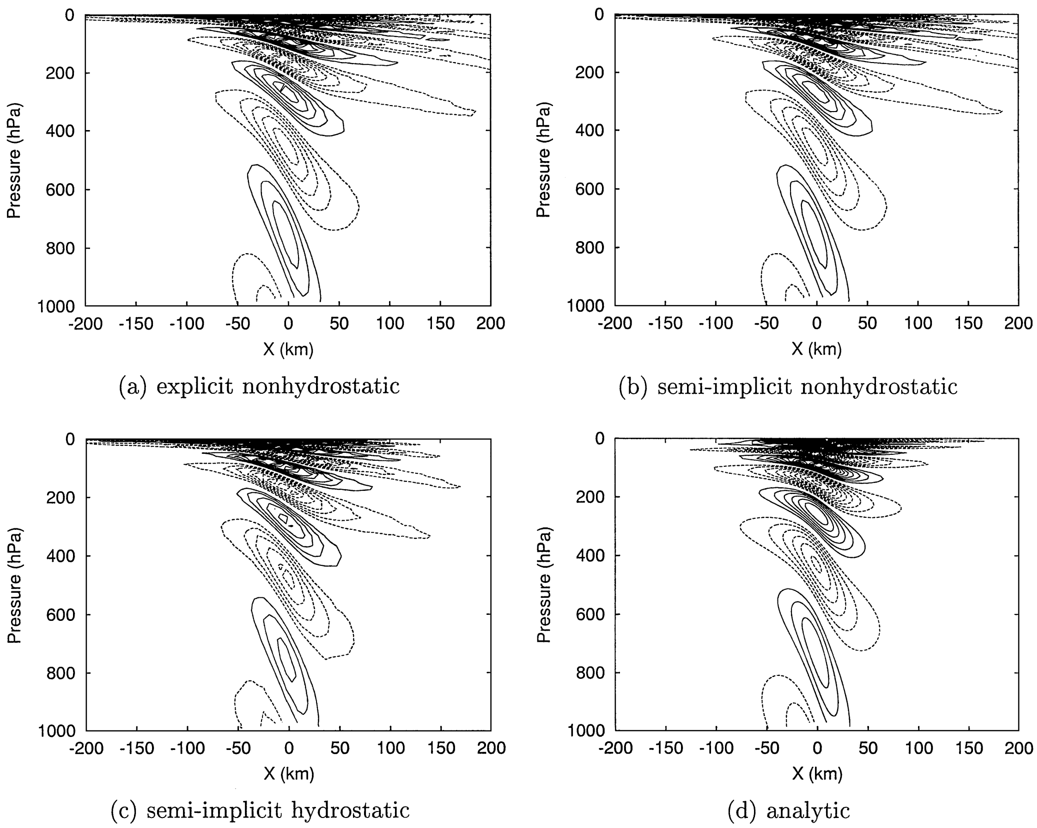

(a) explicit nonhydrostatic

(b) semi-implicit nonhydrostatic

(c) semi-implicit hydrostatic

(d) analytic

Fig. 1. Waves of the vertical velocity field in hydrostatic flow over 2D obstacle. Mountain parameters are $h_0 = 250$ m and $a_x = 30$ km. Isothermal atmosphere with $N = 0.018$ s^{-1} and $U = 25$ m s^{-1}. Contour interval is $\Delta w = 0.05$ m s^{-1}. 114 × 100 × 60 grid with 11 km resolution.

semi-implicit nonhydrostatic and semi-implicit hydrostatic, compared to the semi-analytic solution. The used grid is 206 × 100 points with 11 km horizontal resolution and 60 levels. As it can be seen, the mutual coincidence of the numerical models, as well as the coincidence with the analytical solution, are quite good in the lower and middle atmosphere. In the upper atmosphere the coincidence is also satisfactory. The experiment shows that the developed nonhydrostatic model can adequately simulate hydrostatic flows over mountains.

In the second experiment, presented in Fig. 2, the performance of the model in the linear nonhydrostatic flow regime is investigated. A mountain of 250 m height and half-width $a_x = 2.5$ km is chosen. The atmosphere is characterized by a logarithmic temperature profile with the constant $N = 0.01$ s^{-1} and wind speed $U = 25$ m s^{-1}. The dimensionless flow parameters are $Nh/U = 0.1$ and $Na_x/U = 1$, which characterize the linear nonhydrostatic situation. The model grid is 206 × 100 × 60 with 550 m horizontal resolution, and the integration time is 2000 s. It can be seen that the nonhydrostatic models are almost perfect in representing the flow, giving the right location and amplitude of the cells. As expected, in this highly nonhydrostatic regime the hydrostatic model is not able to catch the downstream tilt of the wave pattern. Its wave amplitude has an inacurate strong growth with height. Due to such a strong growth, the hydrostatic model requires a strong sponge layer and intensive smoothing at the top. In the hydrostatic case, the smoothing intensity by the sponge layer is 7 times stronger than in the nonhydrostatic model. In the case of a more stable stratification, such as in the first experiment, the nonhydrostatic model does not need a sponge layer at all, although a weak

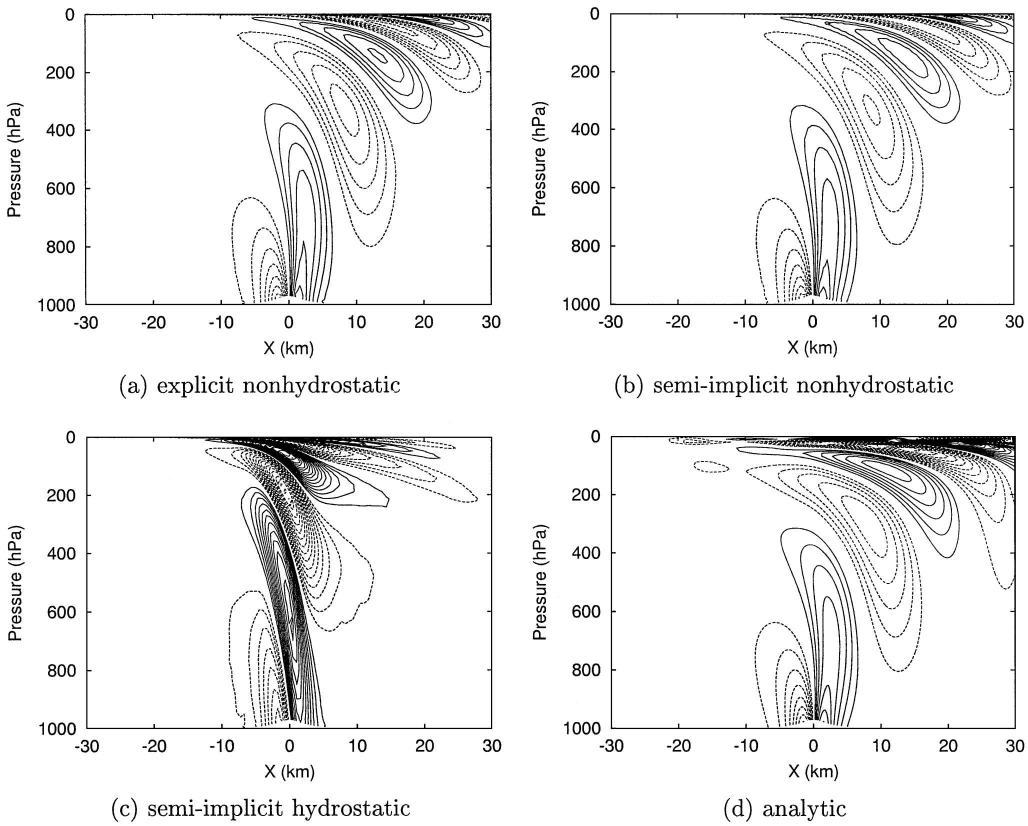

Fig. 2. Waves of the vertical velocity field in nonhydrostatic flow over 2D obstacle. Mountain parameters are $h_0 = 250$ m and $a_x = 2.5$ km. Flow characteristics are $N = 0.01$ s^{-1} and $U = 25$ m s^{-1}. Contour interval is $\Delta w = 0.2$ m s^{-1}. $114 \times 100 \times 60$ grid with 550 m resolution.

damping on the upper level is used in the current experiment.

Note that in the presented figures, the wave patterns are compressed to the top. This is a visible effect of the use of the pressure vertical coordinate. Actually, the vertical wavelength of the stationary orographic waves with constant background stratification is constant in the ordinary physical space. The quality decreases with the height, which is actually determined by the number and location of the vertical numerical discretization levels.

In the third experiment, a simulation of the nonhydrostatic flow over a 3D hill is presented. The characteristics of the flow and grid parameters are the same as for the previous experiment, with the exception that the mountain is finite in the y-direction with $a_y = 2.5$ km. The stability of the atmosphere is characterized by $N = 0.01$ s^{-1} and the wind speed is $U = 25$ m s^{-1}, blowing in the direction of the x-axis. The parameters $Nh/U = 0.1$ and $Na_x/U = 1$ indicate that we have linear nonhydrostatic flow over the mountain.

Figure 3 represents simulations from three different models compared to the analytic solution. The horizontal cross-sections of the vertical wind at 500 mb are given. As can be seen from Fig. 3, both nonhydrostatic models are almost perfect in the simulation of the flow features, while the wave pattern of the hydrostatic model is completely different but still consistent with the theory of hydrostatic flow. Simulation of the flow over a 3D hill should ensure that the model is correct in the representation of dynamics in all dimensions.

The experiments with the artificial orography and the coincidence of their results with exact theoretical solutions allows to one say that the developed nonhydrostatic model is capable of catching nonhydrostatic effects and can be applied for very high-resolution modeling.

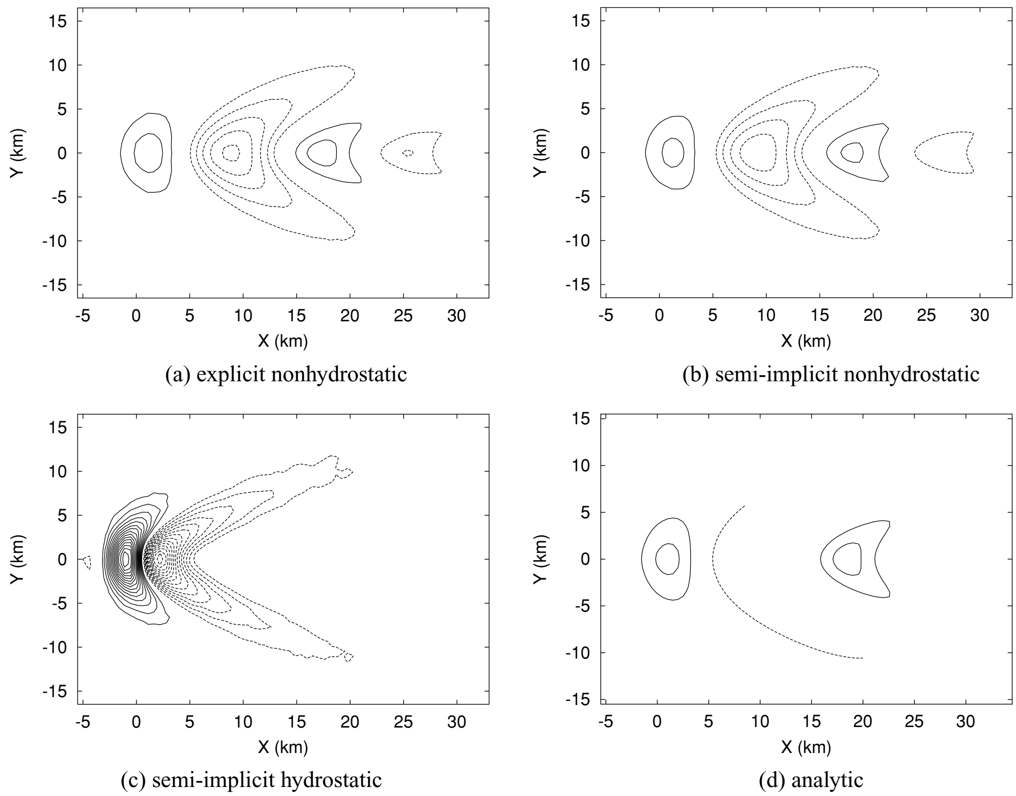

Fig. 3. Horizontal cross-section at 500 hPa of the vertical velocity waves in nonhydrostatic flow over 3D obstacle. Mountain parameters are $h_0 = 250$ m and $a_x = a_y = 2.5$ km. Flow characteristics are $N = 0.01$ s^{-1} and $U = 25$ m s^{-1}. Contour interval is $\Delta w = 0.1$ m s^{-1}. 114 × 100 × 60 grid with 550 m resolution.

3.2. Experiments with real situation

The primary goal of the experiment with the observed data is to show the capabilities of the developed model in a real forecasting situation. The comparison with the hydrostatic original, which has proved its quality in continuous operational forecasting, justifies the assumption that the results are qualitatively reasonable. A test area with a weather situation is selected and the forecasts of different models are compared. At the weather situation selection there was no emphasis on catching the special nonhydrostatic effects, as the physical package of the hydrostatic HIRLAM is not yet tuned for very high-resolution modeling. Meanwhile, significant nonhydrostatic effects are not distinguishable if the grid-step is not small enough. Instead, the focus is on the ability of the model with adjusted surface pressure to produce a reasonable forecast. The modeled event is the development of a fast cyclone of relatively small scale over the Baltic sea. The 24 h forecast is produced with the 11 km resolution model on 114 × 100 × 31 point grid. Time steps during the experiments are 90 s for the hydrostatic semi-implicit, 60 s for the nonhydrostatic explicit and 90 s for the nonhydrostatic semi-implicit models.

In Fig. 4 the sea level surface pressure fields, obtained with the explicit nonhydrostatic, semi-implicit nonhydrostatic and semi-implicit hydrostatic models, are presented. Figure 5 gives cross-sections of the *u*-component of the wind and temperature. The cross-section corresponds to the 14E meridian in Fig. 4.

These figures show a perfect coincidence of all models, although the nonhydrostatic models give a slightly deeper cyclone. Thus, it can be said that the nonhydrostatic models produce reliable results in experiments with real data. Also, these results confirm the applicability of the surface pressure adjustment ideology.

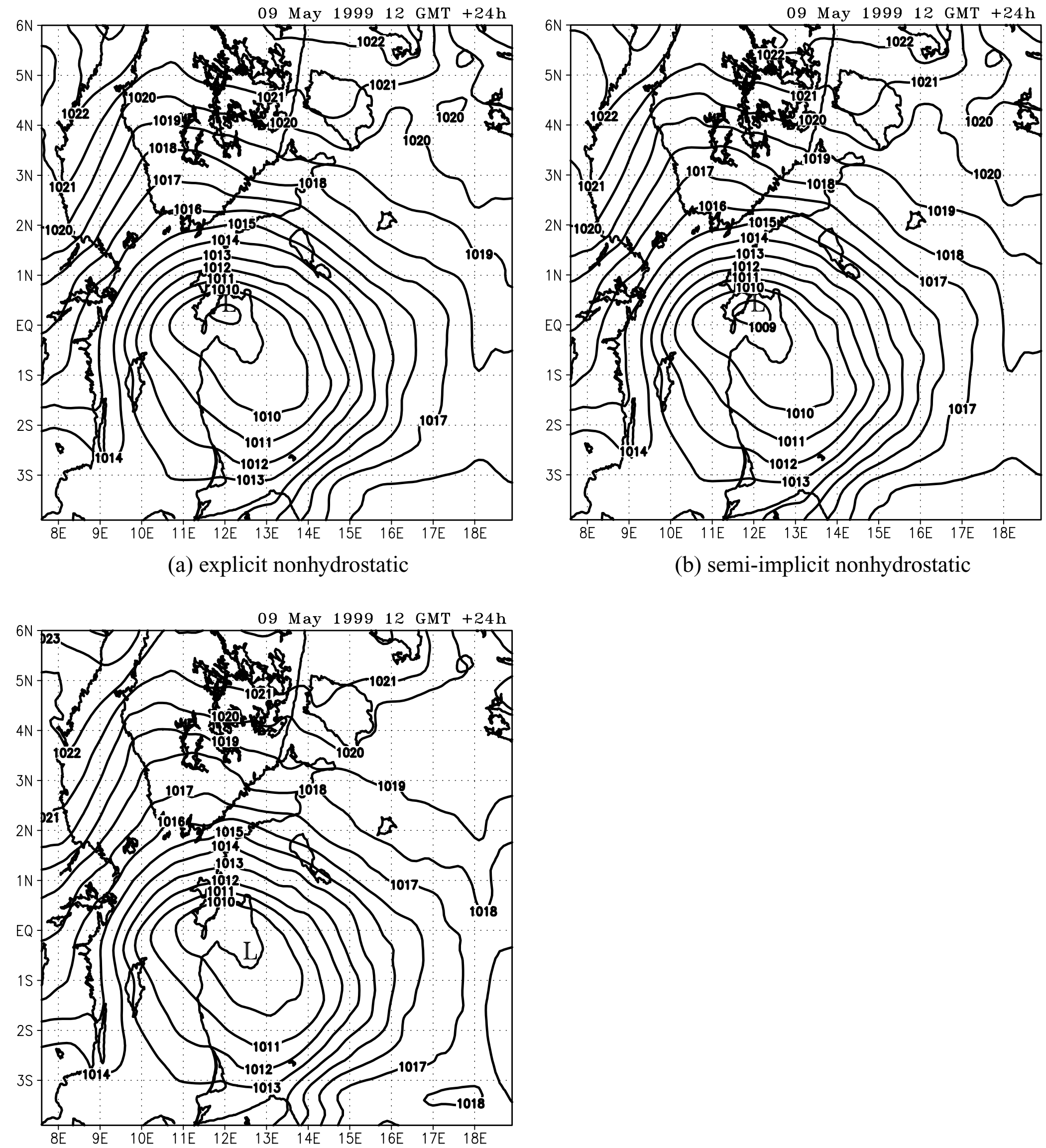

(a) explicit nonhydrostatic

(b) semi-implicit nonhydrostatic

(c) semi-implicit hydrostatic

Fig. 4. 24 h forecast of sea-level pressure with different models. $114 \times 100 \times 31$ grid with 11 km resolution.

4. Conclusions

A solution for the extension of the hydrostatic model into the nonhydrostatic domain is proposed in this paper. The resulting nonhydrostatic model is fully anelastic, filtering both the internal and external sound waves by using the incompressibility of the medium, i.e. the non-divergence of 3D flow in p-space, and surface pressure adjustment. The model does not have explicit boundary conditions for the baric geopotential at the upper and lower boundaries. Instead, the special integral conditions are applied. Cases of the explicit and semi-implicit Eulerian representations are examined. The explicit scheme appears to be a subset of the

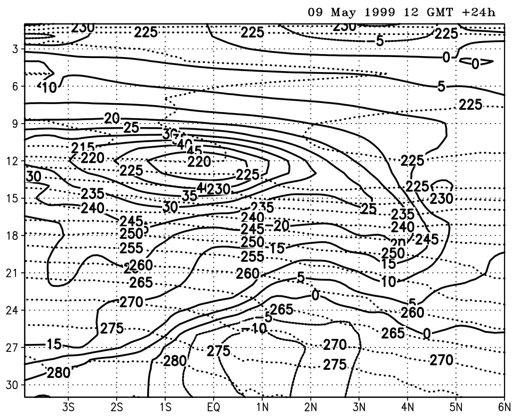

(a) explicit nonhydrostatic

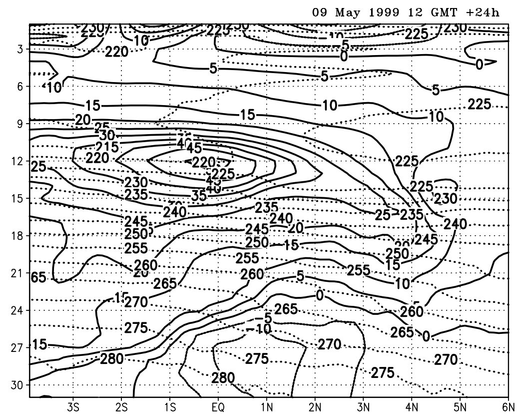

(b) semi-implicit nonhydrostatic

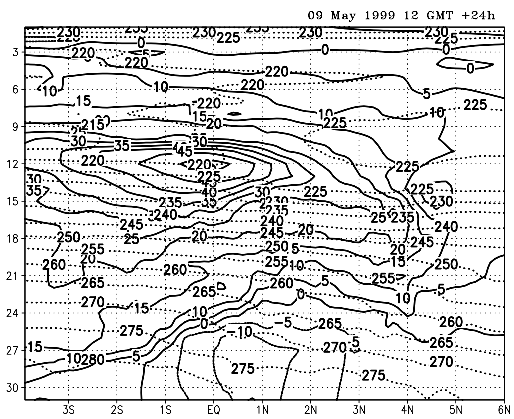

(c) semi-implicit hydrostatic

Fig. 5. 24 h forecast of wind *u*–component (solid) and temperature (dotted) with different models. $114 \times 100 \times 31$ grid with 11 km resolution.

semi-implicit model. The explicit scheme is preferable, when the detailed modeling of buoyancy waves is of special interest.

The nonhydrostatic extension technique is applied in the framework of the HIRLAM numerical weather prediction model, which allows to maintain the existing packages of data assimilation, initialization, nesting and physical routines. The nonhydrostatic model provides HIRLAM with a physically more consistent approach at high-resolution grids.

The model performance is tested in the idealized flow experiments by comparing the nonhydrostatic model with the hydrostatic "parent" model and with the semi-analytic solution. The two- and three-dimensional bell-shaped mountains are used as obstacles in these experiments. The modeling demonstrates that the developed nonhydrostatic model performs correctly in the hydrostatic domain and is able to catch nonhydrostatic phenomena authentically in nonhydrostatic flow regimes.

A real forecast situation was modeled with both the hydrostatic and nonhydrostatic models, and the results were compared. The results show that the developed nonhydrostatic model is capable of working in real operational forecasting conditions. Higher-resolution (2.5 and 1.25 km) experiments are advisable, which, however, require an updated physical package.

The obtained model can be applied in very high-resolution numerical weather prediction. The model is also useful for the scientific development of different parameterization schemes or in the studies of weather systems. In the near future, the nonhydrostatic HIRLAM allows the investigation of weather phenomena down to the cloud scale by nesting the nonhydrostatic model into realistic environmental conditions. In addition, the nonhydrostatic HIRLAM framework provides a good workbench for the comparison of different models, since many different realizations share a common code base.

5. Acknowledgements

The present work was supported by the research Grant 4700 of the Estonian Science Foundation. During his Ph.D. studies A. Männik was supported by the Väisälä Foundation of the Finnish Academy of Sciences and R. Rõõm by the Academy of Finland.

6. Appendix

Derivation of closing terms for the semi-implicit model

The relation for $\Delta_{tt}\omega$ can be obtained from the omega-velocity tendency equation (2.2.12) as follows:

$$\Delta_{tt}\omega = -\Delta t\left(\frac{p}{H^t}\right)^2 \frac{\partial\overline{\phi}^t}{m\partial\eta} + \Delta t F_\omega^t - \omega^t + \omega^{t-\Delta t}. \tag{A.1}$$

To find $\Delta_{tt}\varphi$, the hydrostatic relation (2.2.4) (assuming that R is approximately time-independent) is used:

$$\frac{\partial\Delta_{tt}\varphi}{\partial\eta} = \frac{mR\Delta_{tt}T}{p}. \tag{A.2}$$

From eq. (2.2.2), $\Delta_{tt}T$ is computed as

$$\Delta_{tt}T = \Delta t F_T^t + \Delta t S^t \Delta_{tt}\omega - T^t + T^{t-\Delta t}. \tag{A.3}$$

Finally, integration of eq. (A.2) and substitution from eqs. (A.1) and (A.3) gives for $\Delta_{tt}\varphi$:

$$\Delta_{tt}\varphi = -\,\Delta t^2\int_\eta^1 N^2\frac{\partial\overline{\phi}^t}{\partial\eta}d\eta + R\int_\eta^1(\mu_T + \Delta t S\mu_\omega)\frac{m}{p}\mathrm{d}\eta$$

where

$$\mu_\omega = \Delta t F_\omega^t - \omega^t + \omega^{t-\Delta t},$$

$$\mu_T = \Delta t F_T^t - T^t + T^{t-\Delta t}$$

and

$$N^2 = \frac{RSp}{H^2}.$$

REFERENCES

Arakawa, A. and Lamb, V. R. 1977. Computational design of the basic dynamical process of the UCLA general circulation model. *Meth. Comput. Phys.* **17**, 173–265.

Baines, P. G. 1995. *Topographic effects in startified flows*. Cambridge University Press, New York.

Bubnova, R., Hello, G., Benard, P. and Geleyn, J. F. 1995. Integration of fully elastic equations cast in the hydrostatic pressure terrain-following coordinate in the framework of the ARPEGE/Aladin NWP system. *Mon. Wea. Rev.* **123**, 515–535.

Carpenter, K. M. 1979. An experimental forecast using a nonhydrostatic mesoscale model. *Q. J. R. Meteorol. Soc.* **105**, 629–655.

Davies, H. C. 1976. A lateral boundary formulation for multi-level prediction models. *Q. J. R. Meteorol. Soc.* **102**, 405–418.

Dudhia, J. 1993. A nonhydroatatic version of the Penn State-NCAR mesoscale model: validation tests and simulation of an Atlantic cyclone and cold front. *Mon. Wea. Rev.* **121**, 1493–1513.

Eliassen, A. 1949. The quasi-static equations of motion with pressure as indipendent variable. *Geofys. Publ. (Oslo)* **17**, 1–44.

Laprise, R. 1992. The Euler equations of motion with hydrostatic pressure as an indipendent variable. *Mon. Wea. Rev.* **120**, 197–207.

Laprise, R. and Peltier, W. R. 1989. On the structural characteristics of steady finite-amplitude mountain waves over bell-shaped topography. *J. Atmos. Sci.* **46**, 586–595.

Männik, A. and Rõõm, R. 2001. Non-hydrostatic adiabatic kernel for HIRLAM. Part II. Anelastic, hybrid-coordinate, explicit-Eulerian model. *HIRLAM Technical Report* **49**, 54 pp. Available from the HIRLAM member institutes or http://www.knmi.nl/hirlam/TechReports/TR49ab.html.

Miller, M. 1974. On the use of pressure as vertical coordinate in modeling convection. *Q. J. R. Meteorol. Soc.* **100**, 155–162.

Miller, M. and Pearce, R. P. 1974. A three-dimensional primitive equation model of cumulonimbus convection. *Q. J. R. Meteorol. Soc.* **100**, 133–154.

Robert, A. 1982. A semi-Lagrangian and semi-implicit numerical scheme for the primitive meteorological equations. *J. Meteorol. Soc. Jpn.* **60**, 319–325.

Robert, A. J., Henderson, H. and Turnbull, C. 1972. An implicit time integration scheme for baroclinic modes of the atmosphere. *Mon. Wea. Rev.* **100**, 329–335.

Rõõm, R. 2001. Nonhydrostatic adiabatic kernel for HIRLAM. Part I: Fundametals of nonhydrostatic dynamics in pressure-related coordinates. *HIRLAM Technical Report* **48**, 26 pp. Available from the HIRLAM member institutes or http://www.knmi.nl/hirlam/TechReports/TR48ab.html.

Rõõm, R. and Männik, A. 2002. Non-hydrostatic adiabatic kernel for HIRLAM. Part III. semi-implicit Eulerian scheme. *HIRLAM Technical Report* **55**, 25 pp. Available from the HIRLAM member institutes or http://www.knmi.nl/hirlam/TechReports/TR55ab.html.

Rõõm, R., Miranda, P. and Thorpe, A. 2001. Filtered nonhydrostatic models in pressure related coordinates. *Q. J. R. Meteorol. Soc.* **127**, 1277–1291.

Rõõm[Ryym], R. 1990. General form of the dynamical equations for the ideal atmosphere in the isobaric coordinate system. *Izvestia, Atmos. and Oceanic Phys.* **26**, 9–14.

Salmon, R. and Smith, L. M. 1994. Hamiltonian derivation of the nonhydrostatic pressure-coordinate model. *Q. J. R. Meteorol. Soc.* **120**, 1409–1413.

Simmons, A. J. and Burridge, D. M. 1981. An energy and angular momentum conserving vertical finite difference scheme and hybrid vertical coordinates. *Mon. Wea. Rev.* **109**, 758–766.

Tanguay, M., Robert, A. and Laprise, R. 1990. A semi-implicit semi-Lagrangian fully compressible regional forecast model. *Mon. Wea. Rev.* **118**, 1970–1980.

Tripoli, G. J. 1992. A nonhydrostatic meoscale model designed to simulate scale interaction. *Mon. Wea. Rev.* **120**, 1342–1359.

White, A. A. 1989. An extended version of nonhydrostatic, pressure coordinate model. *Q. J. R. Meteorol. Soc.* **115**, 1243–1251.

Yeh, K.-S., Cote, J., Gravel, S., Methot, A., Patoine, A., Roch, M. and Staniforth, A. 2002. The CMC-MRB Global Environmental Multiscale (GEM) Model. Part III: Nonhydrostatic Formulation. *Mon. Wea. Rev.* **130**, 339–356.